

Influence of Aminosilane Self-assembled Layers on the Adhesion of Electroless Nickel–Phosphorus on a Silicon Wafer

Zi Ting Lin,¹ Chin Ming Chu,¹ Yiu Hsiang Chang,² and Wen Jin Li^{3*}

¹Department of Chemical Engineering, National United University,
No. 1, Lienda, Miaoli 36003, Taiwan, Republic of China

²Department of Chemical Engineering, National Tsing Hua University,
No. 101, Sec. 2, Guangfu Rd., East Dist., Hsinchu 300044, Taiwan, Republic of China

³Material and Chemical Research Laboratories, Industrial Technology Research Institute,
Rm. 804-1, 8F, Bldg. 52, No. 195, Sec. 4, Chung-Hsing Rd., Chutung, Hsinchu 310401, Taiwan, Republic of China

(Received December 30, 2020; accepted April 15, 2021)

Keywords: aminosilane, electroless, adhesion, wafer, Ni-P

Self-assembled layers of aminosilane have been used to bind nanoparticle catalysts for electroless deposition on silicon wafers. However, the influence of accessible amino groups on aminosilane on the adhesion of nickel-phosphorus (Ni–P) deposits has not yet been determined. In this study, we deposited (3-aminopropyl)trimethoxysilane, *N*-(2-aminoethyl)-3-aminopropyltrimethoxysilane, and 3-(trimethoxysilylpropyl)diethylenetriamine as coupling layers between Ni-P films and silicon substrates. We explored the influence of different aminosilanes on the distribution of the catalysts and the adherence of electroless Ni-P films. The surface morphology, composition, and hardness of Ni-P films formed on the different aminosilanes were thoroughly examined. The results indicate that 3-(trimethoxysilylpropyl) diethylenetriamine can bind to the largest number of nanoparticles, but the lack of anchoring sites and catalyst aggregation accounted for the poor adhesion of the Ni-P film deposited on it.

1. Introduction

In the last 10 years, porous silicon has attracted considerable attention because its excellent mechanical properties and large specific surface area make it an ideal material for humidity or gas sensors. To increase the sensing range or selectivity, modification of the porous silicon nanostructure is necessary. Nickel (Ni) binary or ternary alloys deposited through an electroless process are suitable candidates for improving sensor performance.^(1–6) Silicon microchannel plates modified by electroless nickel plating exhibit a faster response and higher sensitivity to vapor humidity than those without electroless plating.⁽¹⁾ The adhesion strength between Ni alloy films and substrates is a key factor influencing the reliability of sensor technologies. To improve adhesion, the deposition of a coupling layer between electroless Ni alloy films and silicon substrates is necessary.

Organosilanes with the general formula (R)₃SiY are potentially effective as coupling layers between Ni alloy films and silicon substrates. Here, R is a hydrolyzable group, such as an alkoxy

*Corresponding author: e-mail: WenJinLi@itri.org.tw
<https://doi.org/10.18494/SAM.2021.3242>

group, that is first hydrolyzed to form the –OH termination, which then reacts with the hydroxyl group on the substrate surface to form the siloxane (Si–O–Si) linkage. Y is an organofunctional group, such as an aminopropyl group, and is used to bind the palladium or nickel catalyst that induces the electroless plating reaction.^(7,8) The catalyst concentration on the smooth surface increases considerably because of the electrostatic interaction and chemical bonding between the catalyst and organosilane layer. The density of palladium nanoparticles distributed on 3-aminopropyl-triethoxysilane (APTES)-modified silicon substrates has been demonstrated to be higher than that on substrates treated with a conventional tin/palladium (Sn/Pd) colloid.⁽⁹⁾ The increased palladium density improves the adherence of electroless plating films on silicon oxide (SiO₂/Si) wafers. When APTES is used to modify a SiO₂/Si wafer, the electroless plating film applied in deep through-silicon vias has favorable conformity and strong adhesion as a barrier layer against copper diffusion.^(9,10)

Self-assembled layers of aminosilanes have been used to bind nanoparticle catalysts for electroless deposition on SiO₂/Si wafers. The influence of the aminosilane structure on deposit adherence is unclear. In this study, we deposited mono-, di-, and tri-aminosilanes as coupling layers between Ni-P and SiO₂/Si substrates. We explored the influence of different aminosilanes on the distribution of the catalysts and the adherence of electroless Ni-P. The surface morphology, composition, and hardness of Ni-P films formed on different aminosilanes were thoroughly examined.

2. Materials and Methods

Silicon <100> wafers coated with a 200-nm-thick SiO₂ layer through chemical vapor deposition (CVD) were used, which were cut into areas of 1 × 2 cm². The substrates were rinsed in deionized (DI) water with a specific resistivity of 18 MΩ-cm, and then rinsed in a sulfuric acid/peroxide mixture solution (97% H₂SO₄: 30% H₂O₂ = 4:1 in volume) at 80 °C for 1 h to remove contaminants. Following several rinses with DI water, the substrates were dipped in heated (80 °C) ammonium hydroxide solution (27% NH₄OH: 30% H₂O₂: H₂O = 1:1:5 in volume) for 30–40 s. Finally, the alkali solution was thoroughly rinsed off with DI water and the substrates were blow-dried using argon gas. Self-assembled layers of aminosilanes were formed on CVD-SiO₂ layers through vapor deposition. Because the aminosilanes used in the study have low vapor pressures, the deposition was performed under a low pressure at 80 °C. The vapor deposition equipment consisted of two separated vacuum chambers and a vacuum pump, as depicted in Fig. 1. The aminosilane was placed in vacuum chamber A and the wafer substrate was placed in chamber B. When the vapor in chamber A reached a steady state, silane was introduced into chamber B. The deposition time was 10–60 min. This process was described in detail in a previous paper.⁽¹¹⁾ Three different aminosilanes were used for the self-assembled layers in this study as depicted in Fig. 2, namely, (3-aminopropyl)trimethoxysilane (1N-silane), *N*-(2-aminoethyl)-3-aminopropyltrimethoxysilane (2N-silane), and 3-(trimethoxysilylpropyl) diethylenetriamine (3N-silane), which were purchased from Sigma-Aldrich. The substrate was subsequently cleaned in ethanol solution to remove excess physisorbed aminosilane molecules. Catalyst immobilization on the substrate was performed by immersing the substrate in a solution

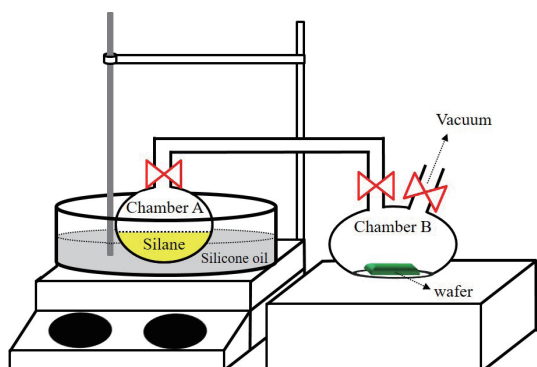


Fig. 1. (Color online) Schematic representation of the aminosilane vapor deposition equipment.

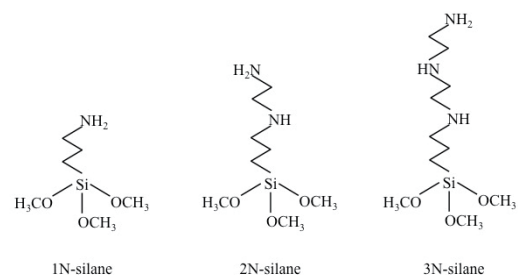


Fig. 2. Schematic structures of (3-aminopropyl)trimethoxysilane (1N-silane), N-(2-aminoethyl)-3-aminopropyltrimethoxysilane (2N-silane), and 3-(trimethoxysilylpropyl)diethylenetriamine (3N-silane).

containing Pd nanoparticles for 20 min. A Pd nanoparticle colloidal solution was fabricated using a reflux-flow system at 360 K for 2 h.⁽¹²⁾ After 1.2 mmol palladium chloride and 5 mmol polyvinylpyrrolidone (PVP) were dissolved in distilled water, formaldehyde was added to the prepared solution as a reductant. The solution's color changed from light yellow to dark brown, indicating the formation of Pd/PVP nanoparticles. PVP was used as the capping molecule to control the nanoparticle size and prevent aggregation.

The Ni-P plating was conducted by dipping the substrate into an electroless plating bath (NICHEM PF-5000, Atotech) in a glass beaker. The bath was heated to 80 °C and stirred moderately with a magnetic stirrer. Stirring was continued during plating to remove bubbles from the substrate.

The surface of modified wafers was characterized through contact angle measurement, X-ray photoelectron spectroscopy (XPS) analysis, and atomic force microscopy (AFM) measurement. The water contact angles were measured using a contact angle goniometer (FTA1000B, First Ten Angstroms, Inc.), which reported the averages of measurements obtained on the aminosilane surfaces at multiple points. XPS was performed with an X-ray photoelectron spectrometer (ESCALAB 250, Thermo Fisher Scientific, Inc.) using a monochromatic Al Kr source and a hemispherical analyzer. AFM measurements were performed using a Digital Instrument Dimension 3100 scanning probe microscope (Advanced Surface Microscopy, Inc.). The nanoparticle distribution on the wafer surface and the morphology of the electroless deposits were characterized using a JEOL-2100 scanning electron microscope (SEM). Cross-sectional observation of the nanoparticles attached to the wafer substrate was performed through high-resolution transmission electron microscopy (HR-TEM) (JEOL JEM-2100F). An energy-dispersive X-ray spectrophotometer (EDX) was used to determine the composition of the electroless deposits. The acceleration voltage and collection time were 20 kV and 100 s, respectively.

A UMIS nanoindenter (Based Model, CSIRO) with a nanoscratch test module and a Berkovich diamond indenter (tip radius ~100 nm, edge angle 130.6°) was used to measure the

interfacial adhesion strength and hardness of Ni-P films deposited on SiO₂/Si wafers. Load control and measurement of the indenter penetration depth were respectively performed using a load cell and a linear variable differential transformer. During indentation tests, the applied load was increased to the maximum value, held at this value, and then released, each for a duration of 30 s. A series of indentations with maximum loads of 1–50 mN were performed. During scratch tests, the load was increased from 0 to 50 mN in 30 s, the scratch length was set as 1500 mm, and the moving velocity was 50 mm/s.

3. Results and Discussion

Water contact angle measurements were performed to evaluate the surface condition at different stages of the surface treatment. The cleaned SiO₂/Si wafer had high hydrophilicity with a water contact angle of less than 10°. When each aminosilane was deposited on the cleaned SiO₂/Si wafer for approximately 10 min, the surface became less hydrophilic and the contact angle was larger than 30°, as shown in Fig. 3. The orientation of NH₂ groups on the wafers determined the wafer hydrophilicity. Some of the terminal NH₂ groups of the aminosilane were oriented toward the inside, so that the hydrophobic alkyl chains were exposed to the outside of the surface.⁽¹³⁾ The wafer modified by 1N-silane was less hydrophilic than those modified by 2N- and 3N-silanes (Fig. 3), which can be attributed to more NH groups being present in the alkyl chains of the 2N- and 3N-silane molecules. The order in which the aminosilane reached a saturated state was 1N-silane > 2N-silane > 3N-silane. After approximately 10 min, the 1N-silane layer bound on the wafer reached a saturated state and the contact angle was maintained at approximately 60°. The saturation time for 3N-silane was longer than 30 min and the contact angle was >50°.

From the XPS results, we determined that the amount of grafted 3N-silane molecules was less than that of grafted 1N-silane molecules after the same deposition time. The N concentrations in the 1N-, 2N-, and 3N-silane layers immobilized on the wafers were

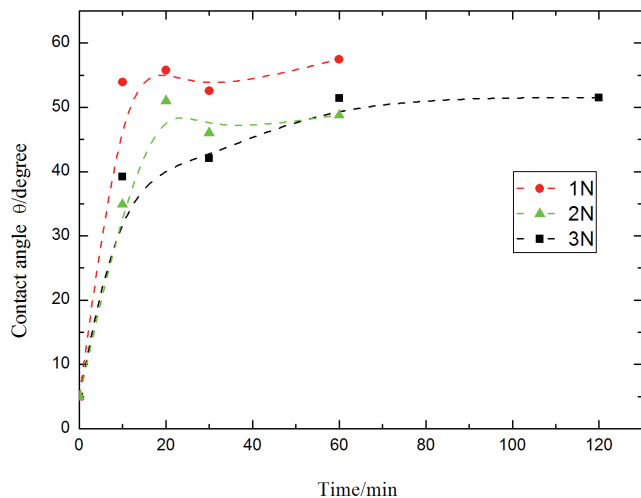


Fig. 3. (Color online) Water contact angle versus deposition time for different aminosilanes.

approximately 2.5, 3.2, and 4.6 atom%, respectively. If the numbers of 2N- and 3N-aminosilane molecules were the same as that of 1N-silane molecules on the SiO₂/Si wafer, the N concentrations in the 2N- and 3N-silane layers would be approximately 4.8 and 7.2 atom%, respectively, as depicted in Fig. 4. The results indicated that the number of aminosilane molecules bound to the silicon substrate was dependent on the alkyl chain length and the number of terminal NH₂ groups. Two possible effects could have influenced aminosilane binding on the wafer. The steric hindrance from the long alkyl chain of the 3N-silane could block subsequent silane molecules from approaching the silicon substrate, extending the 3N-silane saturation time. The other potential influence is that of the protonated amine groups on 3N-silane reacting with hydroxy groups (–OH) on the SiO₂/Si wafer. The XPS spectra for the 1N-, 2N-, and 3N-silanes indicated that the N 1s peaks included two contributions attributed to amine groups (C–NH₂) at 399.3 eV and protonated amines (C–NH₃⁺) at 401 eV. The protonated amine peak indicates that the aminosilane molecules were oriented toward the substrate because of the interaction between the silane NH or NH₂ groups and the OH groups. The 2N- and 3N-silanes had more C–NH₃⁺ than the 1N-silane because of multiple N-groups in the longer alkyl chains, as shown in Table 1. The long alkyl chains oriented toward the substrate reduced the number of free OH groups on the substrate reacting with other aminosilane molecules.

Typical AFM images of aminosilanes deposited on SiO₂/Si wafers are depicted in Fig. 5. The roughness (*Ra*) of the silicon wafer coated with a 200-nm-thick SiO₂ layer through CVD was

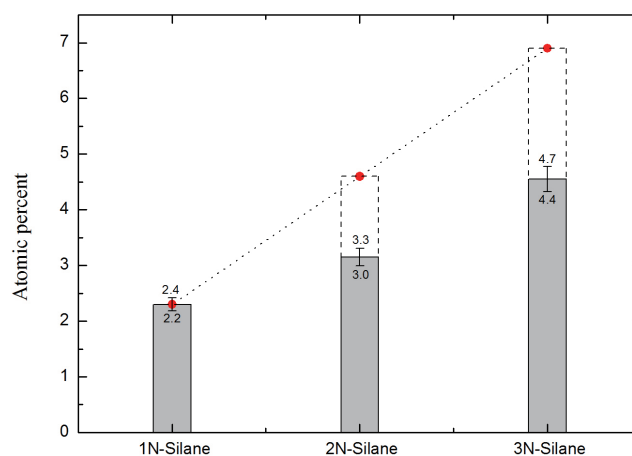


Fig. 4. (Color online) Surface N concentrations (determined through XPS) of different aminosilane layers on SiO₂/Si wafer substrates. Dashed lines indicate the calculated surface N concentration when the number of aminosilane molecules was the same as the number of 1N-silane molecules on the SiO₂/Si wafer.

Table 1
Surface N concentrations (atom%) on the aminosilane-modified SiO₂/Si wafers.

	Composition/atomic percentage	
	NH ₂ (399.3 eV)	NH ₃ ⁺ (401 eV)
1N-silane	1.25	1.05
2N-silane	1.74	1.41
3N-silane	2.89	1.69

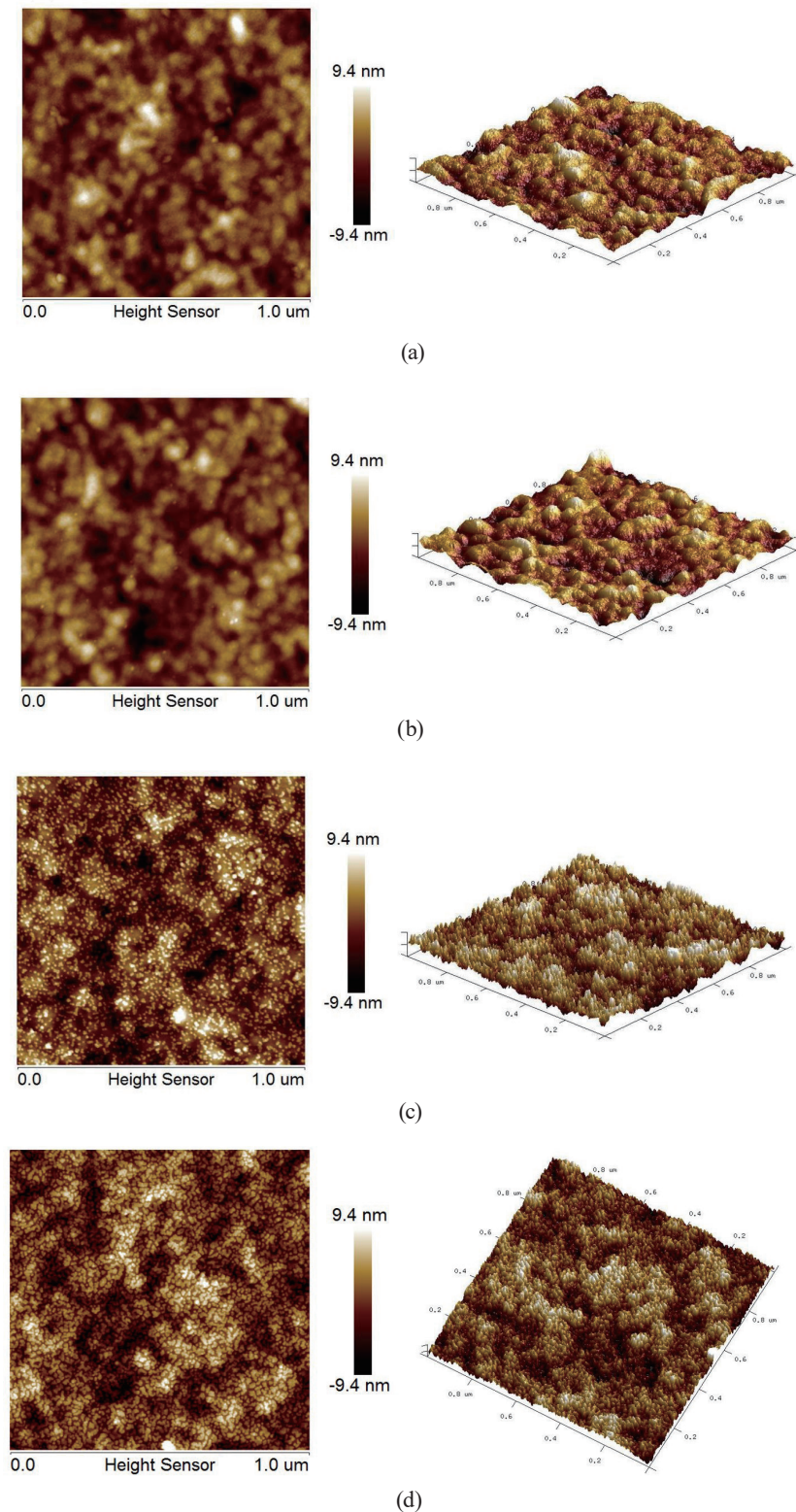


Fig. 5. (Color online) AFM images ($1\ \mu\text{m} \times 1\ \mu\text{m}$) of (a) silicon surface coated with 200 nm SiO_2 (R_a : approximately 1.81 nm); (b) 1N-silane-modified SiO_2/Si wafer (R_a : approximately 2.03 nm); (c) 1N-silane-modified SiO_2/Si wafer after exposure to Pd nanoparticle solution (R_a : approximately 2.60 nm); (d) 3N-silane-modified SiO_2/Si wafer after exposure to Pd nanoparticle solution (R_a : approximately 2.61 nm).

approximately 1.81 nm. Following grafting with aminosilane, the sample roughness (approximately 2.03, 2.60, and 2.61 nm for the 1N-, 2N-, and 3N-silanes, respectively) and the morphology did not markedly change. The silane assembly layer was used as a bridge between the SiO₂ and Pd nanoparticles. The Pd nanoparticles were bound sufficiently strongly because of the electrostatic interaction and coordination bonds between the Pd and N atoms of the amine groups on silane.^(14–16) After immersion in the Pd nanoparticle colloidal solution, numerous tiny protruding structures appeared on the sample surface because of the distribution of Pd nanoparticles over the entire silane layer, as shown in Figs. 5(c) and 5(d). Pd nanoparticle aggregation on 3N-silane was more substantial than that on 1N- or 2N-silane. The SEM image shown in Fig. 6(a) indicates that a high density of Pd nanoparticles was deposited on the 1N-silane-modified wafer with little agglomeration. The density of Pd nanoparticles was 11449 /mm² on the 1N-silane-modified wafer. The SEM image in Fig. 6(b) shows that greater Pd aggregation occurred on the 3N-silane-modified sample, and the density of Pd nanoparticles was 3194 /mm². AFM and SEM revealed that the Pd nanoparticle distribution on the 1N-silane-modified wafer was more uniform than that on the 3N-silane-modified wafer, and the aggregation of Pd nanoparticles was clearly observed on the 3N-silane-modified wafer.

N concentration measurement through XPS revealed that the largest number of charged C-NH⁺ groups were present on the 3N-silane-modified wafer, as listed in Table 1. The synthesized Pd nanoparticles covered with PVP had a negative zeta potential of approximately -11 mV. The positively charged state on the surface was sufficient to enhance Pd nanoparticle adsorption. The ratio of the Pd/Si peaks for different aminosilane-modified wafers indicated that the largest number of Pd nanoparticles were immobilized on the 3N-silane-modified wafer, as shown in Table 2. We hypothesize that the distribution of positive charges was nonuniform on the 3N-silane-modified wafer, which caused nanoparticle aggregation.

Ni-P plating was performed on aminosilane-modified SiO₂/Si wafers in a normal electroless plating bath. A shiny appearance was observed for all samples after 3 min deposition. The EDX results indicated that the composition of Ni-P was not significantly affected by the different amino self-assembled layers bound to the SiO₂. The P concentration was approximately 12 wt% in the films. A SEM image depicting the surface morphology of the as-deposited Ni-P film on

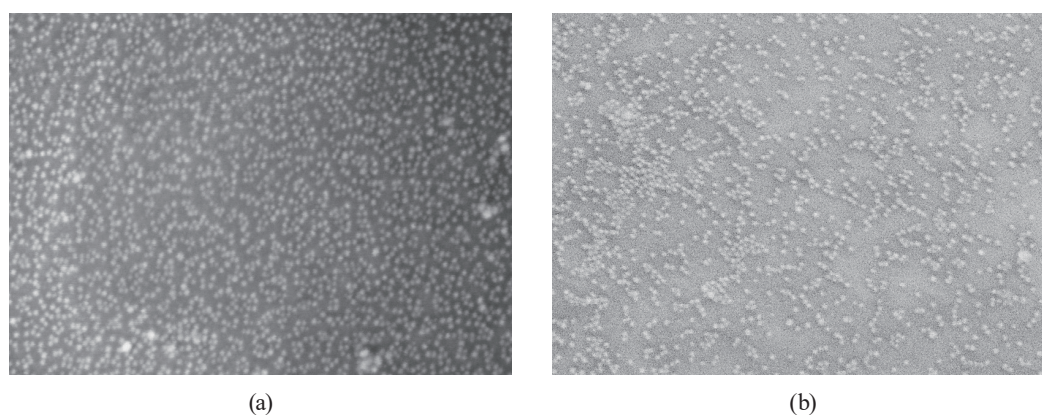


Fig. 6. (Color online) SEM images of Pd nanoparticles on different aminosilane-modified SiO₂/Si wafers. (a) 1N-silane; (b) 3N-silane.

the 1N-silane-modified wafer is shown in Fig. 7(a). A smooth surface with some nodules, possibly introduced by the aggregation of Pd nanoparticles, was established on the silicon wafer substrate. Some grooves and cracks were noted in the Ni-P film deposited on the 3N-silane-modified wafer, as presented in Fig. 7(b). The aggregation and nonuniform distribution of Pd nanoparticles resulted in uneven deposition on the 3N-silane-modified SiO₂/Si wafer. Rapid reduction reactions occurred on the Pd aggregation area, causing the Ni-P film in this region to become thick and exhibit defects due to hydrogen evolution. Thus, the high stress on the Ni-P film caused cracking in weak spots.

The adhesion and hardness of the Ni-P films deposited on different aminosilane layers were measured using the nanoscratch test. The hardnesses of the Ni-P films deposited on 1N-, 2N-, and 3N-silane layers were 5.84, 5.94, and 4.92 GPa, respectively. The adhesion of the Ni-P film deposited on the 3N-silane layer was markedly poorer than that of the Ni-P films deposited on the 1N- and 2N-silane layers. The measured critical loads of the Ni-P films on the 1N- and 2N-silane-modified substrates were approximately 20 and 15.45 nN, respectively. The critical load of the Ni-P/3N-silane samples was too small to measure through a nanoscratch test. The as-deposited Ni-P films on the 3N-silane layers sometimes peeled off easily when rinsed with DI water. This poor adhesion of the Ni-P film deposited on the 3N-aminosilane layer may be caused by two factors, which are explained as follows:

1. Although more -NH₂ and -NH groups were present to interact with the Pd nanoparticles for the 3N-silane, the XPS results indicated that the number of 3N-silane molecules bound on the wafers was lower than that of 1N-silane molecules. Therefore, the number of anchoring sites

Table 2

Average N/Si and Pd/Si composition ratios in the aminosilane-modified SiO₂/Si wafers following immersion in a Pd nanoparticle colloidal solution.

	Average composition ratios	
	N/Si	Pd/Si
1N-silane	0.101	0.232
2N-silane	0.143	0.353
3N-silane	0.155	0.393

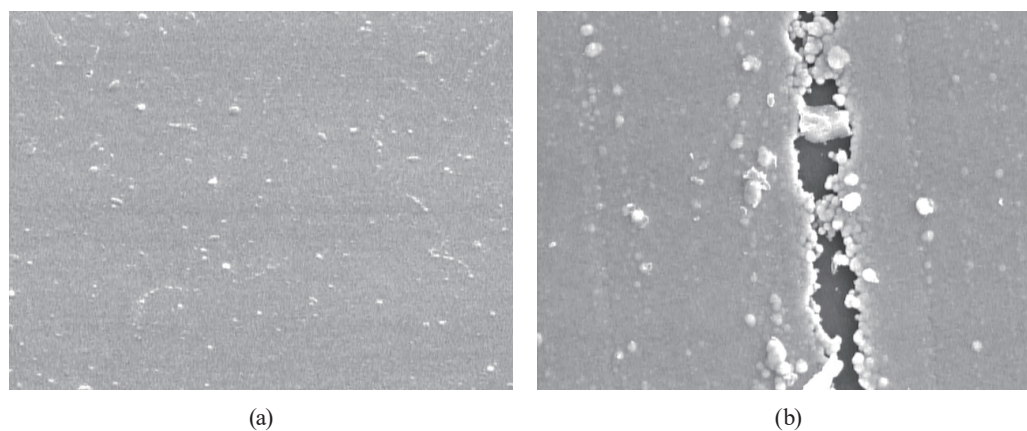


Fig. 7. (Color online) SEM images of Ni-P films deposited on different aminosilane-modified SiO₂/Si wafers. (a) 1N-silane; (b) 3N-silane.

(Si–O–Si) formed by 3N-silane molecules was not sufficient to support deposition. The adhesion of Ni-P films on different aminosilane-modified wafers was in the order 1N > 2N > 3N.

2. The Ni-P film deposited on the 3N-silane-modified wafer exhibited high internal stress, causing weak adhesion. Hydrogen incorporated in the deposited Ni-P films was observed in the regions of Pd aggregation on the 3N-silane-modified substrate. The incorporation of hydrogen in the coating is one major reason for the increase in internal stress.⁽¹⁷⁾ When the internal stress was larger than the strength of the interaction between the Ni-P films and the substrate, the deposited films cracked.

4. Conclusion

Aminosilane self-assembled layers bound to SiO₂/Si wafers are suitable coupling layers for immobilizing Pd nanoparticles. We found that electroless Ni-P deposition was initiated by these immobilized Pd nanoparticles, and Ni-P films were deposited stably on wafers as sensitivity enhancers for humidity sensors. The long alkyl chains of 2N- or 3N-silane on the substrate interfered with the subsequent binding; thus, the packing density of 2N- or 3N-silane on the wafer was lower than that of 1N-silane under the same conditions. The nonuniform distribution of Pd-NPs observed on the 3N-silane-modified wafer created aggregation regions that initiated electroless plating with a short time lag, resulting in nonuniform deposition and subsequent cracks. The use of 1N-silane as a coupling layer most effectively hastened electroless Ni-P deposition. An insufficient number of anchoring sites (Si–O–Si) were formed using 3N-silane, and thus the adhesion of Ni-P on the wafer was weak. The composition of the Ni-P film on the SiO₂/wafer was not affected by silanization with various types of aminosilanes.

References

1. F. Miao, B. Tao, L. Sun, J. You, L. Wang, and P. K. Chu: *Sens. Actuators, A* **160** (2010) 48. <https://doi.org/10.1016/j.sna.2010.03.010>
2. B. Tao, J. Zhang, F. Miao, H. Li, L. Wan, and Y. Wang: *Sens. Actuators, B* **136** (2009) 144. <https://doi.org/10.1016/j.snb.2008.10.039>
3. S. Ozdemir, J. L. Gole: *Sens. Actuators, B* **151** (2010) 274. <https://doi.org/10.1016/j.snb.2010.08.016>
4. J. Kanungo, C. Pramanik, S. Bandopadhyay, U. Gangopadhyay, L. Das, H. Saha, and R. T. T. Gettens: *Semicond. Sci. Technol.* **21** (2006) 264. <https://doi.org/10.1088/0268-1242/21/7/023>
5. H. Y. Wang, Y. Q. Wang, Q. F. Hu, and X. J. Li: *Sens. Actuators, B* **166–167** (2012) 451. <https://doi.org/10.1016/j.snb.2012.02.087>
6. J. I. A. Rashid, J. Abdullah, N. A. Yusof, and R. Hajian: *J. Nanomater.* **2013** (2013) 328093. <https://doi.org/10.1155/2013/328093>
7. A. N. Vasiliev, L. V. Golovko, V. Trachevsky, G. S. Hall, and J. G. Khinast: *Microporous Mesoporous Mater.* **118** (2009) 251. <https://doi.org/10.1016/j.micromeso.2008.08.026>
8. L. Xu, J. Liao, L. Huang, D. Ou, Z. Guo, H. Zhang, C. Ge, N. Gu, and J. Liu: *Thin Solid Films* **434** (2003) 121. [https://doi.org/10.1016/S0040-6090\(03\)00274-8](https://doi.org/10.1016/S0040-6090(03)00274-8)
9. F. Inoue, T. Shimizu, H. Miyake, R. Arima, T. Ito, H. Seki, Y. Shinozaki, T. Yamamoto, and S. Shingubara: *Electrochim. Acta* **82** (2012) 372. <https://doi.org/10.1016/j.electacta.2012.04.165>
10. A. Ikeda, A. Sakamoto, R. Hattori, and Y. Kuroki: *Thin Solid Films* **517** (2009) 1740. <https://doi.org/10.1016/j.tsf.2008.09.068>
11. F. Zhang, K. Sautter, A. M. Larsen, D. A. Findley, R. C. Davis, H. Samha, and M. R. Linford: *Langmuir* **26** (2010) 14648. <https://doi.org/10.1021/la102447y>

- 12 S. Yagi, T. Ashida, T. Nomoto, H. Namatame, and M. Taniguchi: *J. Surf. Anal.* **14** (2008) 444.
- 13 A. K. Chauhan, D. K. Aswal, S. P. Koiry, S. K. Gupta, J. V. Yakhmi, C. Surgers, D. Guerin, S. Lenfant, and D. Vuillaume: *Appl. Phys. A* **90** (2008) 581. <https://doi.org/10.1007/s00339-007-4336-7>
- 14 W. J. Dressick, C. S. Dulcey, J. H. Georger Jr., G. S. Calabrese, and J. M. Calvert: *J. Electrochem. Soc.* **141** (1994) 210. <https://doi.org/10.1149/1.2054686>
- 15 L. Xu, J. Liao, L. Huang, D. Ou, Z. Guo, H. Zhang, C. Ge, N. Gu, and J. Liu: *Thin Solid Films* **434** (2003) 121. [https://doi.org/10.1016/S0040-6090\(03\)00274-8](https://doi.org/10.1016/S0040-6090(03)00274-8)
- 16 N. E. Cant, K. Critchley, H. L. Zhang, and S. D. Evans: *Thin Solid Films* **426** (2003) 31. [https://doi.org/10.1016/S0040-6090\(02\)01300-7](https://doi.org/10.1016/S0040-6090(02)01300-7)
- 17 C. S. Lin, C. Y. Lee, F. J. Chen, and W. C. Li: *J. Electrochem. Soc.* **152** (2005) 370. <https://doi.org/10.1149/1.1901064>